Research Paper

Muscle xenografts reproduce key molecular features of facioscapulohumeral muscular dystrophy

Amber L. Mueller[a], Andrea O'Neill[a], Takako I. Jones[b], Anna Llach[a,1], Luis Alejandro Rojas[c], Paraskevi Sakellariou[a,d], Guido Stadler[e,2], Woodring E. Wright[e], David Eyerman[c], Peter L. Jones[b], Robert J. Bloch[a,*]

[a] Department of Physiology, University of Maryland, Baltimore, 655 W, Baltimore St., Baltimore, MD 21201, United States of America
[b] Department of Pharmacology, University of Nevada, Reno School of Medicine, 1664 North Virginia Street, Reno, NV 89557, United States of America
[c] Fulcrum Therapeutics, 26 Landsdowne St., Cambridge, MA 02139, United States of America
[d] FAME Laboratory Department of Exercise Science, University of Thessaly, Karies, Trikala 42100, Greece
[e] Department of Cell Biology, UT Southwestern Medical Center Dallas, TX 75390, United States of America

ARTICLE INFO

ABSTRACT

Aberrant expression of *DUX4*, a gene unique to humans and primates, causes Facioscapulohumeral Muscular Dystrophy-1 (FSHD), yet the pathogenic mechanism is unknown. As transgenic overexpression models have largely failed to replicate the genetic changes seen in FSHD, many studies of endogenously expressed *DUX4* have been limited to patient biopsies and myogenic cell cultures, which never fully differentiate into mature muscle fibers. We have developed a method to xenograft immortalized human muscle precursor cells from patients with FSHD and first-degree relative controls into the *tibialis anterior* muscle compartment of immunodeficient mice, generating human muscle xenografts. We report that FSHD cells mature into organized and innervated human muscle fibers with minimal contamination of murine myonuclei. They also reconstitute the satellite cell niche within the xenografts. FSHD xenografts express *DUX4* and DUX4 downstream targets, retain the 4q35 epigenetic signature of their original donors, and express a novel protein biomarker of FSHD, SLC34A2. Ours is the first scalable, mature *in vivo* human model of FSHD. It should be useful for studies of the pathogenic mechanism of the disease as well as for testing therapeutic strategies targeting *DUX4* expression.

1. Introduction

Facioscapulohumeral muscular dystrophy-1 (FSHD) is a common autosomal dominant muscular dystrophy, affecting approximately 1 in 8333 humans, that is caused by the loss of repression at the D4Z4 repeats locus at the telomeric end of chromosome 4q. Healthy individuals have 11–100 D4Z4 repeated units within the 4q35 region, whereas individuals with FSHD have only 1–10 D4Z4 units (van Deutekom et al., 1993; Lemmers et al., 2002). This contraction alters the local epigenetic environment and makes the region more accessible to transcription machinery, resulting in the aberrant transcription of genes that are not normally expressed in muscle. For disease to occur, a full-length double homeobox 4 (*DUX4*) mRNA must be transcribed from the last D4Z4 repeat unit (RU) in the contracted array and polyadenylated using the polyadenylation signal of the 4qA haplotype distal to the array (Lemmers et al., 2002; Gabriels et al., 1999; Tupler and Gabellini, 2004; Lemmers et al., 2010). The expression of DUX4 protein in muscle is correlated with muscle cell death (Geng et al., 2011) and the development of FSHD (Snider et al., 2010), yet the mechanisms linking an increase in DUX4 to muscle degeneration remain poorly understood.

Many laboratories have attempted to delineate the pathogenic mechanism of DUX4 in FSHD. As DUX4 is a transcription factor,

considerable effort has focused on the discovery of the genes that it activates, including *ZSCAN4*, *TRIM43*, *MBD3L2* and others (Ferreboeuf et al., 2014; Geng et al., 2012). To date, however, there is no clear explanation as to how low levels or sporadic expression of DUX4 or the downstream genes it targets cause myopathy (Tassin et al., 2013). In fact, recent reports suggest that, in rare cases, low levels of *DUX4* can be expressed by genetically normal myonuclei without the D4Z4 genetic contraction (Jones et al., 2012). Furthermore, 1–2% of the human population has a contracted D4Z4 region and 4qA haplotype but never develops FSHD (Tupler and Gabellini, 2004; Ricci et al., 2014). These results suggest that pathological modifiers of DUX4 or its downstream targets, or additional pathogenic factors encoded by the D4Z4 region, have yet to be discovered.

Although many potential biomarkers of FSHD have been identified in *in vitro* studies of FSHD muscle cells (Jagannathan et al., 2016) and muscle biopsies, the pathophysiological role of DUX4 and its gene targets has yet to be studied in an *in vivo* humanized model. This is because the derepressed *DUX4* retrogene is unique to primates (Snider et al., 2010; Clapp et al., 2007). Much of the seminal data on FSHD was collected using immature human myocytes and myotubes in culture (Tassin et al., 2013; Dixit et al., 2007; Xu et al., 2014; Stadler et al., 2011; Himeda et al., 2014), but cultured muscle cells do not recapitulate many features of adult muscle fibers. Additionally, some investigators have used viral overexpression of *DUX4* in the *tibialis anterior* (TA) muscles of mice to cause dystrophy (Wallace et al., 2011; Wallace et al., 2012), but the *DUX4* levels achieved in these studies were far greater than those seen in FSHD patients. One group created a transgenic mouse by chromosomal insertion of contracted D4Z4 regions, but the mouse failed to recapitulate the dystrophic phenotype (Krom et al., 2013). Recent studies in the Jones laboratory have focused on a murine model in which very low levels of DUX4 are expressed unless the gene is intentionally upregulated (Jones and Jones, 2018). Although each of these models has provided pivotal insight into the molecular basis of DUX4 toxicity, the activation of DUX4's downstream genes in mouse muscle is different from that in human muscle (Sharma et al., 2013). Thus, even mouse models in which the levels of *DUX4* expression is comparable to that in FSHD muscle (Jones and Jones, 2018; Bosnakovski et al., 2017), are of limited physiological relevance.

As an alternative to approaches that express DUX4 in murine muscles, we and others have turned to xenografting human muscle tissue (Chen et al., 2016; Zhang et al., 2014) or muscle precursor cells (Sakellariou et al., 2016) into the hindlimbs of mice. Although the two approaches differ in key respects, they each have the advantage of creating mature human muscle tissue in mice and each has been shown to be compatible with studies of FSHD. Our approach, the injection of immortalized human muscle precursor cells (hMPCs) from an FSHD patient donor or a healthy relative, result in human muscle xenografts that recapitulate normal muscle biology. Here we further characterize our xenograft model.(Sakellariou et al., 2016) and demonstrate its usefulness for studies of FSHD. Notably, the xenografts of FSHD but not control cells replicate in mature skeletal muscle tissue the genetic and epigenetic differences seen in biopsies and cell lines. Moreover, the FSHD xenografts show early evidence of pathology, including a key biomarker of disease.

2. Results

2.1. FSHD and control muscle engraftment is enhanced by iNMES

To generate a humanized model of FSHD in mice, we developed methods to grow human muscle within the TA compartment of the mouse hindlimb from immortalized human muscle precursor cells (hMPCs, Appendix A, S. Fig. 1) (Sakellariou et al., 2016). The hMPCs were developed from primary cultures prepared from biceps muscle of an individual carrying a D4Z4 genetic contraction to leave 4 RUs in one FSHD-permissive 4qA allele (FSHD) or a first-degree unaffected relative

with two non-permissive 4qB alleles (control) (Jones et al., 2012; Rahimov et al., 2012). For these studies we chose individual subclones of each characterized cell line (Jones et al., 2012; Homma et al., 2012), which were then immortalized by transfection with hTERT and CDK4 (Stadler et al., 2011), termed 15Abic (FSHD) and 15Vbic (control).

To create the human muscle xenografts, we first prepared a niche to seed the hMPCs within the TA of the mouse hindlimb. We X-irradiated the hindlimbs of 8-week-old immunodeficient NRG mice, to prevent the regeneration of the murine muscle at later times. Six days later we injected cardiotoxin along the length of the TA to eliminate much of the mouse muscle tissue. The following day we injected 2×10^6 hMPCs and allowed the muscle to develop over the next 4 weeks. During that period, we performed intermittent neuromuscular electrical stimulation (iNMES) of the peroneal nerve to induce repeated maximal contractions of the engrafted TA muscles (Sakellariou et al., 2016). At 4–5 weeks post-engraftment, we dissected the TA muscles for comprehensive analysis. Details are provided in Appendix B. Supplemental Methods and Appendix A. S. Fig. 1.

Fig. 1a shows cross sections of iNMES-treated xenografts formed by FSHD and control hMPCs that were immunolabeled with an antibody specific for human β-spectrin (green), to visualize the sarcolemma of fibers of human origin, and a non-species-specific desmin antibody (red) to co-label all fibers. We counted the number of human fibers per graft from each experimental group (control, $n = 16$; control + iNMES, $n = 13$; FSHD, $n = 20$; FSHD + iNMES, $n = 15$). As we reported previously (Sakellariou et al., 2016), iNMES treatment significantly increased the number of human myofibers formed in the xenografts, by both control and FSHD cells (Fig. 1b). By comparing the TA weights upon dissection, we found that while iNMES increased the number of human muscle fibers within the xenografts, it did not alter the average weight of the TA muscles as a whole (Appendix A. S. Fig. 2b & c), suggesting that the untreated xenografts may contain more connective or adipose tissue than iNMES-treated grafts. To test this, we fluorescently stained cross sections of FSHD and control grafts, with and without iNMES treatment, with wheat germ agglutinin (WGA), an extracellular matrix marker (Appendix A. S. Fig. 3a), and BODIPY (493/503) which labels lipid droplets (Appendix A. S. Fig. 3b), along with our human specific antibodies (Emde et al., 2014; Spangenburg et al., 2011). We see greater WGA labeling in the unstimulated control and FSHD cross sections (Appendix A. S. Fig. 3a, magenta) indicating greater fibrosis, but no differences in BODIPY staining (SI Fig. 3b, green). Thus, fibrosis, and not fat content or adipocytes, is reduced by iNMES in both control and FSHD xenografts.

To quantify the sizes of the muscle fibers with and without iNMES, we measured the minimum Feret's diameter of each human muscle fiber in our xenografts (Briguet et al., 2004). In xenografts formed by either FSHD or control hMPCs, iNMES significantly increased the average diameter of the human fibers (Fig. 1c). The distribution plots of fiber diameter (Appendix A. S. Fig. 4a) in iNMES treated-grafts are right-shifted and wider than the untreated controls, consistent with iNMES promoting fiber growth. Notably, even without iNMES the average diameters of FSHD and control fibers still fall within a physiologic range (Briguet et al., 2004). We also measured the distance between the largest muscle fibers within each graft and the nearest human fibers and found that iNMES significantly decreased this distance in controls grafts (Appendix A. S. Fig. 4b & c). As the fibers within the unstimulated FSHD xenografts were more compact than the controls, iNMES treatment had only a modest effect. We attribute this difference to greater fibrosis in the interstitial space between fibers, which was most apparent in unstimulated control xenografts (Appendix A. S. Fig. 3a). We also quantified the number of human myonuclei per human fiber in our grafts, as indicated by the presence of human lamin A/C within or in the interstitial space surrounding human fibers (h-β-spectrin) (Appendix A. S. Fig. 4d,e). We did not see any significant differences in nuclei/fiber or percent interstitial nuclei in any of our experimental groups.

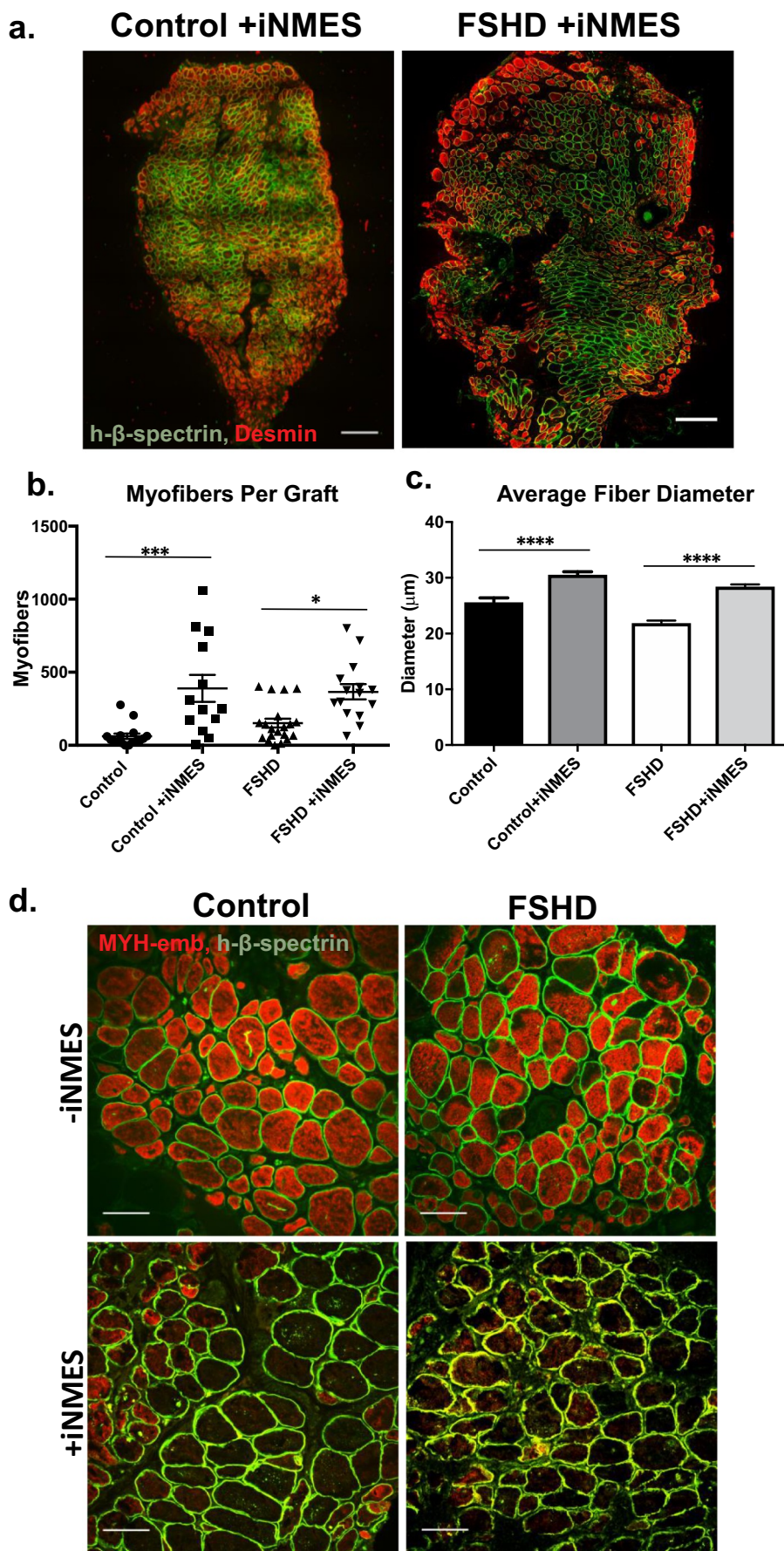In addition to increasing fiber size and improving tissue

Fig. 1. iNMES increases human muscle fiber number, diameter, and differentiation in FSHD and control xenografts. (a) Cross sections of TA muscles carrying xenografts of control and FSHD hMPCs after iNMES were immunolabeled with antibodies to h-β-spectrin (green; sarcolemma of human fibers) and co-labeled with antibodies to desmin (red; human and murine myofibers; bars = 200 μm). (b) Human myofibers, labeled with anti-h-β-spectrin, were counted per xenograft within each group (control, $n = 16$; control + iNMES, $n = 13$; FSHD, $n = 20$; FSHD + iNMES, $n = 15$). iNMES increased the number of human fibers formed in both FSHD ($P < .012$) and control ($P < .0002$) grafts. Each data point represents an individual xenograft. Lines show means ± SEM. (c) Engrafted fiber diameters were measured with FIJI. Data are means + SEM. Control + iNMES fibers ($n = 385$) were larger than control ($n = 214$, $P < .0001$) fibers and FSHD + iNMES fibers were larger than FSHD fibers ($P < .0001$). One-way ANOVA with Tukey's multiple comparisons tests were used for (b) and (c). See Appendix C. S. Table 1 for all *P*-values. *$P < .05$, ***$P < .001$, ****$P < .0001$. (d) Human fibers within cross sections of control (left) or FSHD (right) xenografts were labeled with anti-h-β-spectrin (green) and antibodies to embryonic myosin heavy chain (MYH-emb, red). iNMES treatment (lower panels) reduced expression of embryonic myosin, indicating greater maturation. Bars = 50 μm. (For interpretation of the references to colour in this figure legend, the reader is referred to the web version of this article.)
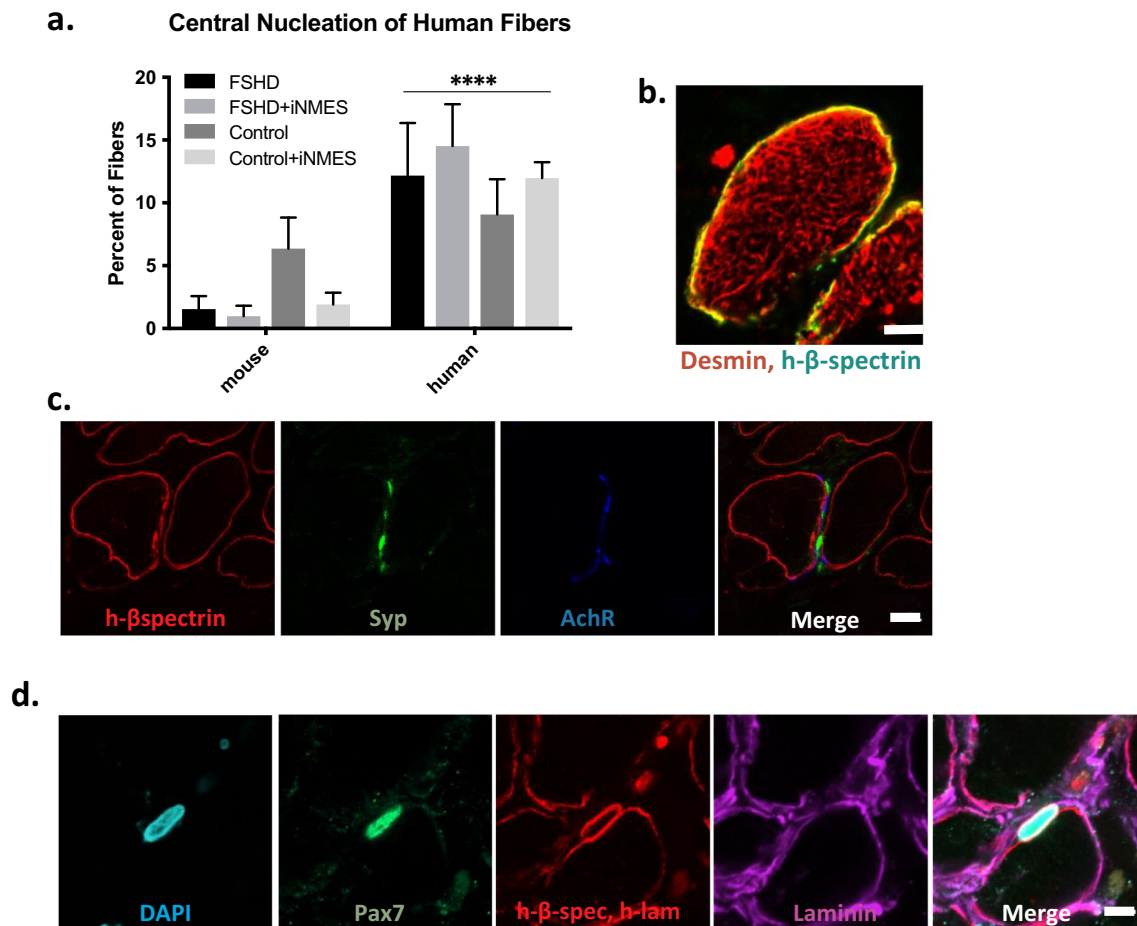
Fig. 2. Mature properties of FSHD xenografts. (a) We labeled frozen cross sections of FSHD and control xenografts with antibodies to h-β-spectrin and h-lamin A/C and counterstained with DAPI to label all nuclei. We identified all CNFs and counted human and murine central nuclei, identified as those nuclei that did or did not label for h-lamin A/C, respectively. CNFs, mouse or human, were expressed as a percentage of the number of human fibers. Data are means ± SEM (control, $n = 11$; and control + iNMES, $n = 13$; FSHD, $n = 9$; FSHD + iNMES, $n = 10$). There were significantly more human CNFs than mouse CNFs when comparing all groups, mouse *vs* human (****$P < .0001$). None of the differences within the mouse group or human group were significant (Two-way ANOVA with Bonferroni's multiple comparisons test; see Appendix C. S. Table 2 for P-values). (b) A representative image of a cross section of an FSHD fiber from a graft subjected to iNMES and labeled with anti-h-β-spectrin (green) and anti-desmin (red). Desmin within a human fiber showed a reticular pattern, indicating mature organization of desmin filaments. Bar = 5 μm. (c) NMJs in an FSHD graft after iNMES treatment were labeled with α-bungarotoxin (AchR, blue; the postsynaptic membrane), and antibodies to h-β-spectrin (red; the human sarcolemma), and synaptophysin (Syp, green; presynaptic terminals). Bar = 10 μm (d) A representative image of a human satellite cell in an FSHD xenograft after iNMES. DAPI (blue) was used to label the nucleus of a mononuclear cell, which co-labeled with antibodies to the satellite cell marker, PAX7 (green). This cell's nuclear envelope labeled with anti-h-lamin A/C (red) and was adjacent to a human muscle fiber (anti-h-β-spectrin, also red) within the basal lamina (labeled with antibodies to laminin, purple), defining it as a human satellite cell. Bar = 5 μm. (For interpretation of the references to colour in this figure legend, the reader is referred to the web version of this article.)

organization, iNMES treatment significantly enhanced muscle fiber differentiation, as shown by a reduction of the levels of embryonic myosin (MYH-emb), labeled by immunofluorescence (Fig. 1d, red). Combined, these data suggest that iNMES induces the development and maturation of both control and FSHD muscle xenografts within the mouse hindlimb.

2.2. Xenografts are primarily human in origin and morphologically mature

In earlier studies of engraftment of human myoblasts into mouse skeletal muscle, the grafts were partially contaminated by host myonuclei, likely due to fusion of donor cells with resident host fibers (Quenneville et al., 2007; Fakhfakh et al., 2012a; Fakhfakh et al., 2012b). To minimize this, we used high dose (25 Gy) X-irradiation to suppress murine myogenesis and thereby to favor the formation of human muscle tissue with minimal murine myonuclear contamination. To test for murine myonuclei in the human myofibers in our xenografts, we immunolabeled cross sections with antibodies to human lamin A/C

(h-lamin A/C) at the nuclear envelope, as well as with antibodies to human β-spectrin (h-β-spectrin), and counterstained with DAPI. We counted all centrally nucleated fibers (CNFs) and determined if each central nucleus labeled for h-lamin A/C. Those that remained unlabeled were counted as mouse central nuclei. These results were expressed as a percentage of total fibers that were centrally nucleated with either human or mouse myonuclei (Fig. 2a). As in our previous report (Sakellariou et al., 2016), mouse CNFs were present in < 2% percent of the total fibers in FSHD, FSHD + iNMES, and control + iNMES xenografts (1.6%, 0.98%, and 1.9%, respectively). In unstimulated control xenografts mouse CNFs comprised a higher (6.4%) percentage of the total fibers, but this difference was not significant. Human CNFs are present in 9–15% of all engrafted fibers, significantly higher than mouse CNFs in all xenograft groups (all human CNFs v. all mouse CNFs $P < .0001$; see Appendix C. Table 2 for statistical comparisons of each experimental group). Thus, all xenografts (FSHD and control, +/− iNMES) were primarily of human origin and were minimally contaminated by murine myonuclei.
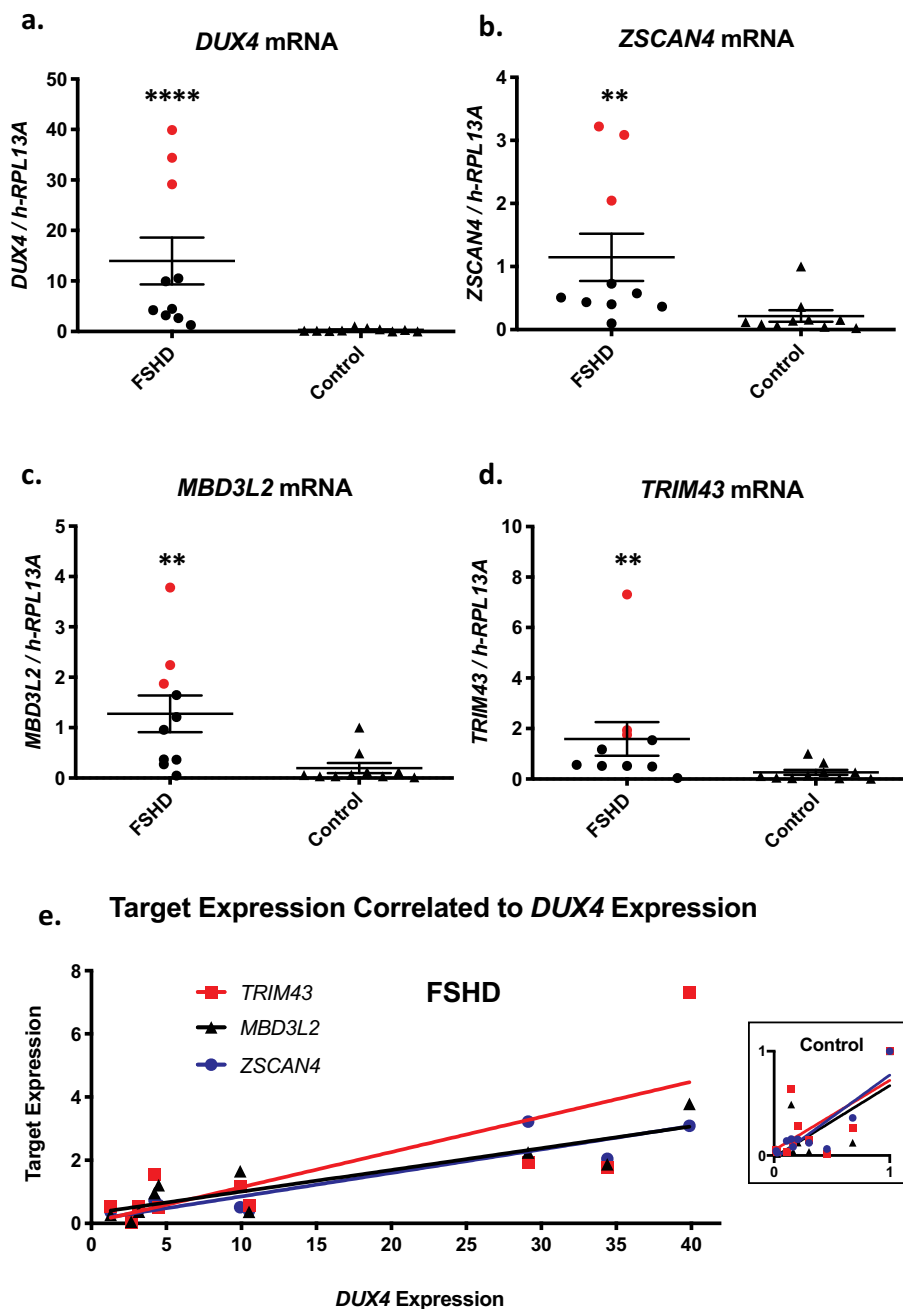
a. *DUX4* mRNA

b. *ZSCAN4* mRNA

c. *MBD3L2* mRNA

d. *TRIM43* mRNA

e. Target Expression Correlated to *DUX4* Expression

Fig. 3. FSHD xenografts express *DUX4* and DUX4 target genes in a *DUX4*-dependent manner. Nested qPCR was used with mRNA from TA muscles carrying FSHD and control xenografts to measure levels of *DUX4* mRNA and mRNA encoding three of DUX4's downstream targets (*n* = 10 each). (a) *DUX4* expression was greater in FSHD xenografts compared to controls (P < .0001), with three xenografts expressing relatively high levels of *DUX4* (red). (b-d) mRNA encoding DUX4 targets, *ZSCAN4*, *MBD3L2* and *TRIM43*, was greater in FSHD xenografts compared to controls (P < .0029, P < .0039, P < .0089, respectively). Red data points indicate results from the same 3 grafts, which had the highest levels of *DUX4* and its targets across all assays (a-d). Lines within the scatter plots indicate means ± SEM. The Mann-Whitney *U* test was used for (a-d). (e) DUX4 target expression linearly correlated with *DUX4* expression. R^2 values from linear regression analyses of *DUX4* to *ZSCAN4* (blue), *TRIM43* (red), and *MBD3L2* (black) in FSHD grafts are 0.85, 0.60, and 0.77, respectively. **P < .01, ****P < .0001. (For interpretation of the references to colour in this figure legend, the reader is referred to the web version of this article.)
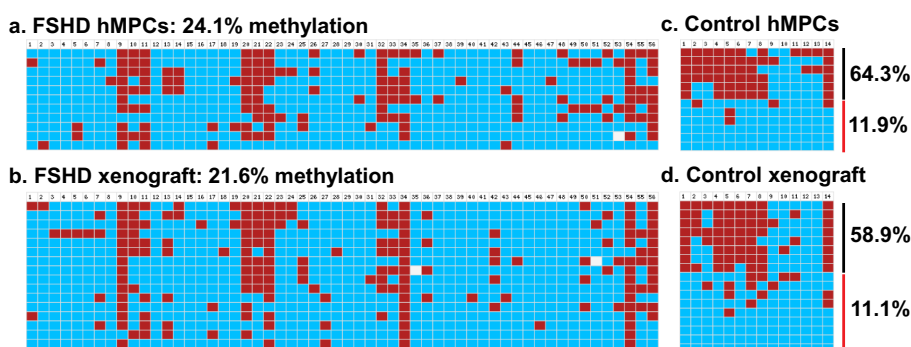
a. FSHD hMPCs: 24.1% methylation

b. FSHD xenograft: 21.6% methylation

c. Control hMPCs

d. Control xenograft

Fig. 4. FSHD and control sequences maintain epigenetic signature through culture and engraftment. Representative BSS analysis of the distal D4Z4 RU on the contracted 4qA allele (BSSA) in a) FSHD hMPCs and b) an FSHD xenograft, and the distal D4Z4 RUs of the long (black bar) and short (red bar) 4qB alleles (BSSB) in c) control hMPCs and d) a control xenograft. The BSSA assay analyzed 56 CpGs (columns) and the BSSB assay analyzed 16 CpGs (columns) from 12 independent chromosomes (rows). Red squares indicate methylated CpG, blue squares indicate unmethylated CpGs, and white squares indicate that the expected CpG was missing. Percent methylation for each sample is indicated (see SI Table 3 for more information). (For interpretation of the references to colour in this figure legend, the reader is referred to the web version of this article.)

To further assess the structural organization of the muscle tissue in the xenografts, we immunolabeled cross sections with anti-h-β-spectrin (green) and with anti-desmin (Fig. 2b, red). The reticular staining for desmin, evident in fibers in all xenografts, indicates that this filament system is organized around the myofibrils, as in mature muscle fibers (Capetanaki et al., 2007). Another feature that defines mature skeletal muscle is intact neuromuscular junctions (NMJs). Human fibers in cross sections were immunolabeled with anti-h-β-spectrin (Fig. 2c, red), while presynaptic vesicles and post-synaptic acetylcholine receptors (AchR) were labeled with antibodies to synaptophysin (Syp, green) and α-bungarotoxin (blue) to visualize the junctions. Both FSHD and control grafts contained fibers innervated by mouse motor neurons at NMJs. This is consistent with our morphometric observations of +iNMES xenografts, which are robust and fully differentiated, properties which would have been significantly altered in the absence of innervation. These results indicate that engrafted FSHD and control hMPCs mature into organized and innervated human muscle fibers.

Next, we examined the xenografts to learn if the satellite cell niches in controls and FSHD muscles were repopulated by engrafted hMPCs. Fig. 2d shows a mononuclear cell within the basement membrane (labeled with anti-laminin, purple) and outside the sarcolemma of a human muscle fiber (stained with anti-h-β-spectrin, red). The cell's nucleus is immunofluorescently labeled with anti-h-lamin A/C (also red) and the satellite cell marker PAX7 (green), which defines it as a satellite cell of human origin. This suggests that the hMPCs are capable not only of developing into muscle fibers but also of repopulating the satellite cell niche within the TA compartment of mice. We obtained similar results when we examined control xenografts and we never observed non-human (h-lamin A/C-negative) PAX7-positive satellite cells within our xenografts, which is likely an outcome of our use of high dose X-irradiation. These results suggest that both control and FSHD xenografts have the potential to regenerate after injury from their respective human populations of satellite cells.

2.3. FSHD xenografts express DUX4 and DUX4 targets

The molecular hallmark of FSHD is the aberrant expression of DUX4 and its downstream targets, which is linked to a decrease in CpG methylation in the D4Z4 region (Lemmers et al., 2002; Gabriels et al., 1999; Tupler and Gabellini, 2004; Lemmers et al., 2010; Snider et al., 2010; Daxinger et al., 2015; van Overveld et al., 2003; Zeng et al., 2009; Yao et al., 2014). We quantified *DUX4* expression by RT-qPCR in FSHD and control xenografts with the most human fibers (iNMES does not significantly alter *DUX4* expression in FSHD grafts: Appendix A. S. Fig. 5a), and normalized to human *RPL13A* expression, to eliminate any contribution of murine mRNA. FSHD xenografts expressed significantly higher amounts of *DUX4* mRNA compared to controls (Fig. 3a, $P < .0001$). *DUX4* mRNA expression was not directly correlated to fiber number or nuclei per fiber number (Appendix A. S. Fig. 5b, c), supporting the idea that *DUX4* is pathologically expressed in a sporadic and/or transient manner in a small population of FSHD myonuclei (Tassin et al., 2013). We used the same technique to quantify the expression of several DUX4 target genes. Expression of *ZSCAN4*, *MBD3L2*, and *TRIM43* was significantly higher in FSHD xenografts than controls (Fig. 3b, $P < .0029$; Fig. 3c, $P < .0039$; Fig. 3d, $P < .0089$). Notably, *DUX4* expression in the FSHD xenografts was not normally distributed, as three xenografts showed high levels, whereas 7 other grafts showed much lower levels (Fig. 3a, red). The same three xenografts with high *DUX4* levels expressed the highest levels of mRNA of several of DUX4's target genes, (Fig. 3b–d, red), suggesting that DUX4, while variable among FSHD samples, upregulates each target proportionately. When target expression was correlated to the expression of *DUX4*, strong linear relationships were observed in the FSHD grafts (Fig. 3e). R^2 values from linear regression analyses of *DUX4* expression to expression of *ZSCAN4*, *TRIM43*, and *MBD3L2* were 0.85, 0.60, and 0.77, respectively. Control xenografts expressed very low levels of *DUX4* and the targets

(Fig. 3a–d) and showed poorer correlations (Fig. 3e, insert; *ZSCAN4* $R^2 = 0.77$; *TRIM43* $R^2 = 0.43$; *MBD3L2* $R^2 = 0.46$). These results indicate that our FSHD model recapitulates the changes in gene expression that occur in FSHD.

2.4. Xenografts reproduce the epigenetic features of patients with FSHD

FSHD is also characterized by DNA hypomethylation of the contracted chromosome 4qA D4Z4 array, with fewer repeats and lower levels of methylation generally correlating with a more severe disease phenotype (Snider et al., 2010; van Overveld et al., 2003; Zeng et al., 2009; Balog et al., 2012; Jones et al., 2014). We used bisulfite sequencing (BSS) to assay the DNA methylation profiles in the distal D4Z4 RUs for the 15Abic FSHD (4qA/B) and 15Vbic control (4qB/B) hMPCs and xenografts. In Fig. 4, each column represents a CpG site for potential DNA methylation, while each row represents a linear chromosome from an independent cell culture or xenograft. The hMPCs used to generate the FSHD grafts were hypomethylated (24.1% methylation) on the contracted 4qA allele (Fig. 4a), similar to the levels measured in the primary cells used for immortalization (Jones et al., 2015). FSHD xenografts were similarly hypomethylated (21.6% methylation) in the same distal D4Z4 RU (Fig. 4b), indicating the pathogenic epigenetic status was retained in the xenograft. Methylation analysis of the control hMPCs and xenografts required a different BSS assay, as they do not contain a 4qA allele and therefore the sequence of the DNA analyzed was from both 4qB alleles. In addition, the two 4qB alleles in 15Vbic hMPCs and xenografts have two epigenetic populations (Fig. 4c,d, black & red lines). The methylation profiles showed the expected hypermethylation of the expanded 4qB allele (black lines) and hypomethylation of the contracted 4qB allele (red lines) Importantly, these profiles were similar between the hMPCs and the xenografts, consistent with earlier results with biopsies (Himeda et al., 2016). Thus, the xenografts of control and FSHD cells have epigenetic profiles similar to the muscles biopsied from control and FSHD patients.

2.5. FSHD xenografts are phenotypically distinct from controls

In addition to the molecular and epigenetic features of FSHD recapitulated in our xenografts, we have identified SLC34A2 as a gene product that is up-regulated in the FSHD grafts compared to controls. *SLC34A2* encodes the sodium-dependent phosphate transport protein 2B, an ion co-transporter (Su et al., 2004), and is a known DUX4 target (Geng et al., 2012; Rahimov et al., 2012). We counted the number of fibers that were immunofluorescently labeled with antibodies to SLC34A2 in cross sections (Fig. 5a, red) that colabeled for h-β-spectrin (Fig. 5a, green). In intact fibers, SLC34A2 labeling was limited to human fibers and labeled in a reticular pattern, indicating its probable localization to the one or more of the internal membrane systems in muscle fibers (Fig. 5a). We also observed several SLC34A2-positive fibers that appeared to be in various states of necrosis (Appendix A. S. Fig. 6a-d). We measured an average of 1.4% ± 0.3 of FSHD fibers that immunolabeled for SLC34A2, compared to 0.12% ± 0.07 of control fibers (Fig. 5e, $p < .029$). A value of 1.4% of fibers is in the range in which DUX4 is expressed pathologically (Tassin et al., 2013). Congruent with this increase in protein expression, *SCL34A2* mRNA is also present at higher levels in FSHD grafts than in controls (Fig. 5c). We examined cross sections from 6 paired FSHD patient and control biceps biopsies and confirmed the presence of SLC34A2-positive fibers in 4 of the 6 FSHD samples, which showed no other obvious signs of muscle wasting (Fig. 5d, red; Appendix A. Fig. 6 f-h, green). We observed no such fibers in any of the 6 healthy control patient samples. SLC34A2-positive fibers were rare (< 1 per 14mm^2) in these otherwise healthy-looking FSHD cross sections. SLC34A2 labeling may therefore serve as a surrogate biomarker for DUX4 expression in future studies of FSHD pathogenesis and of potential therapies to treat the disease.
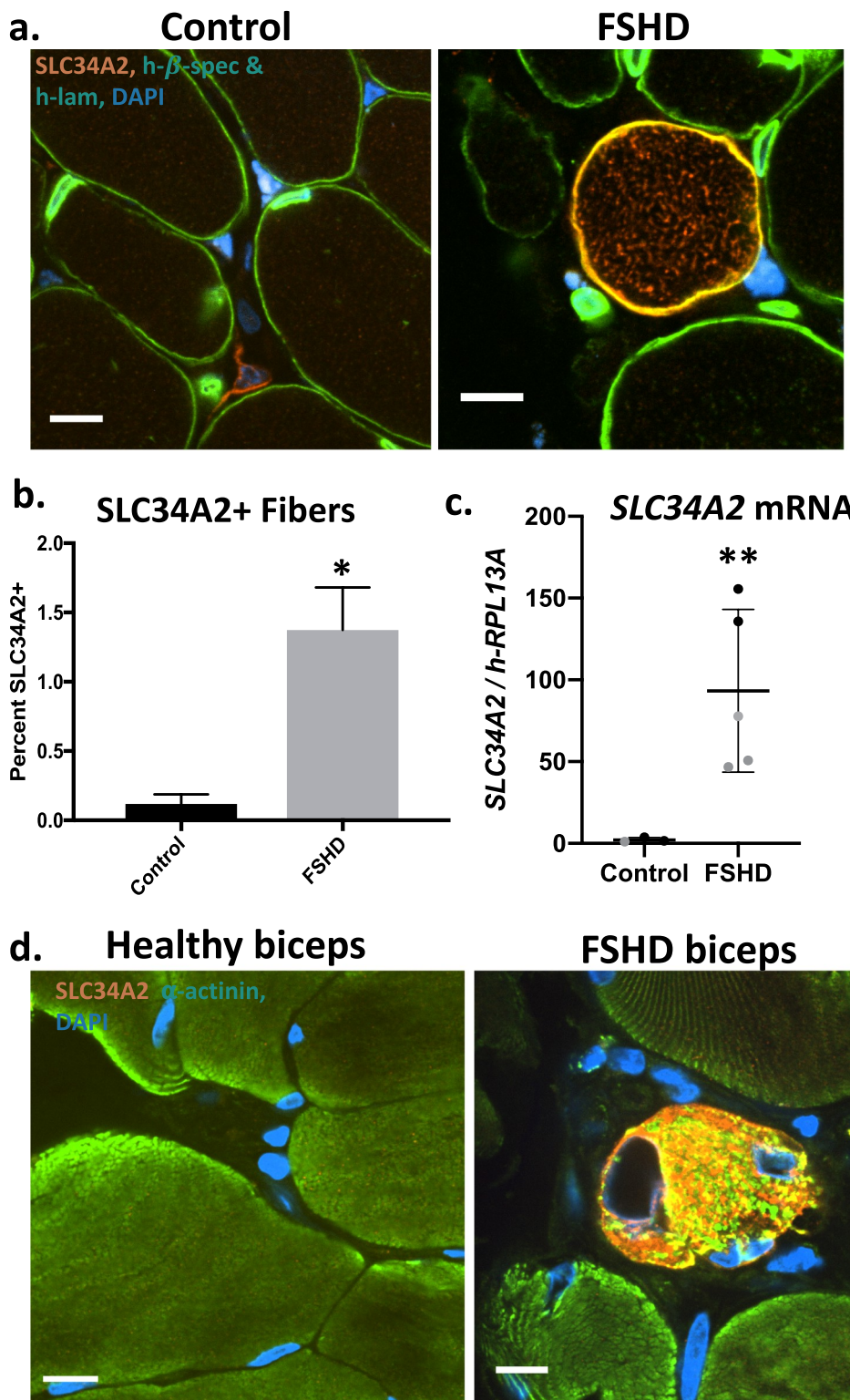
Fig. 5. Increased expression of a protein biomarker, SLC34A2, distinguishes FSHD from control xenografts. (a) Antibodies to SLC34A2 (red), h-β-spectrin (green) and h-lamin A/C (green), as well as DAPI, were used to label FSHD and control xenografts. Bar = 10 μm. (b) Fibers expressing SLC34A2 were counted and displayed as a percentage of total human fibers within each xenograft type (n = 4 each). FSHD grafts had more fibers expressing SLC34A2 than controls (mean + SEM; P < .0286, Mann-Whitney U test). (c) qPCR was used with mRNA from TA muscles carrying FSHD (n = 5) and control xenografts (n = 3) to measure levels of *SLC34A2* mRNA. *SLC34A2* was upregulated 47-fold in FSHD grafts compared to controls (mean ± SD; unpaired *t*-test with Welch's correction, P < .01). Black points represent results from qPCR analysis performed in triplicate. Grey points represent results from qPCR analysis from single reactions (due to limited sample). If only data from points analyzed in triplicate are used for statistics, *P* = .04. (d) SLC34A2 (red) positive fibers in an FSHD biceps biopsy. DAPI and anti-α-actinin identified nuclei and muscle fibers, respectively. All fibers in the cross section of control biceps were SLC34A2 negative. Bars = 10 μm. *P < .05, **P < .01. (For interpretation of the references to colour in this figure legend, the reader is referred to the web version of this article.)

3. Discussion

Although xenografts of dissociated cells have been commonly used in the study of other diseases, such as cancer, their use in the study of muscular dystrophies has been limited, typically because the efficiency of engraftment is low (Quenneville et al., 2007). Here we address the challenge of creating a mouse model carrying mature FSHD muscle. We show that mature human muscle tissue can form in immunocompromised mice without significant contamination of the human myofibers by murine myonuclei, and that the grafts that form from immortalized muscle cells from an FSHD patient are just as robust as those from a healthy, first-degree relative. We show further that the FSHD and control grafts are composed of innervated, differentiated myofibers and satellite cells that are human in origin. Perhaps most importantly, they exhibit the same biomarkers and genetic and epigenetic properties as the parent cell lines and the biopsies from which those cells were first derived. Thus, our approach to xenografting yields FSHD and control muscle tissues in the mouse hindlimb that are very

similar to the tissues of patients and their close relatives.

An alternative approach to xenografting involves transplanting small bundles of fibers from fresh muscle biopsies from FSHD patients into mice (Chen et al., 2016; Zhang et al., 2014). This approach has been used successfully to test an siRNA that reduces expression of *DUX4* and its downstream targets (Chen et al., 2016). The major disadvantage of engrafting fiber bundles is that a biopsy must be taken for each round of engraftment and only a limited number of mice can be engrafted from each biopsy. Thus, it is not "scalable", *i.e.*, it cannot generate the numbers needed for large-scale testing of therapeutics. Having sufficient numbers of mice, analyzed in an unbiased fashion, is key to successful tests that can be independently reproduced and on which translational studies can be based. By contrast, our approach is scalable and reproducible, as it uses immortalized clonal myogenic cells from FSHD patients and their first-degree relatives, which are available in essentially unlimited numbers.

We were particularly excited to find satellite cells of human origin within our xenografts. This result is intriguing because it shows that not only are the hMPCs able to generate myofibers in the mouse, but they are also able to repopulate the satellite cell niche in mature skeletal muscle, as reported by others (Ehrhardt et al., 2007). This indicates that the xenografts replace mouse muscle and include the precursor population for muscle turnover in the engrafted TA compartment. In future studies we plan to challenge the engrafted muscle with a myotoxin and large strain injury (Roche et al., 2010; Roche et al., 2012; Roche et al., 2015) to compare repair and regeneration of FSHD to control muscle.

Another benefit of the xenograft model of FSHD is that it can be used to study the epigenetic component of pathogenesis. Because the grafts retain the same CpG methylation signature as their respective donors and maintain all the endogenous regulatory aspects of the intact human locus, we can test therapeutic strategies to alter the epigenetic status to ameliorate the disease. For example, treatments that upregulate or increase the activity of DNA methyltransferase 3B, which is responsible for repressing chromatin within the D4Z4 region (van den Boogaard et al., 2016), or those that knock down expression of candidate chromatin remodeling genes functioning at the pathogenic allele (Himeda et al., 2018), could be tested using our model.

In addition to the epigenetics of FSHD replicated in our model, FSHD grafts express endogenous *DUX4* and DUX4 targets that can be measured reliably by qPCR. In fact, the relative variability in *DUX4* expression in our model replicates the variability of *DUX4* expression seen in FSHD patient biopsies (Snider et al., 2010). Importantly, we see high degrees of linear correlation between *DUX4* and the DUX4 targets, *ZSCAN4, MBD3L2* and *TRIM43*. Thus, our model likely reflects a larger range of FSHD phenotypes which may depend on the level of *DUX4* expression. Subsequent studies with xenografts may be able to attribute phenotypic differences or variable disease severity to the level of *DUX4* or DUX4 target expression. Therefore, this model should be particularly useful for testing therapies aimed at reducing *DUX4* expression and assessing potential off-target effects of drugs in FSHD muscle.

DUX4 enrichment is reported to occur in < 5% of myonuclei in human-derived FSHD myotubes in culture (Tassin et al., 2013), and many fewer DUX4-positive myonuclei are likely present in mature muscle tissue. Due to the rarity of DUX4 expression and its transient nature, the protein has been very difficult to detect reliably in western blot or immunofluorescence, emphasizing the need for surrogate biomarkers of disease. Here, we describe a novel protein biomarker which is readily identified in FSHD xenografts but not in controls, SLC34A2. SLC34A2 protein is very rarely detectable by immunofluorescence labeling in control xenografts but increases 10-fold in FSHD xenografts. *SCL34A2* mRNA increases 47-fold, as measured by RT-qPCR. It is likely that increased SLC34A2 expression, which is upregulated in FSHD biopsies and primary myoblasts as part of the DUX4 pathway (Geng et al., 2012; Rahimov et al., 2012), marks fibers in which DUX4 is expressed. Although we must confirm that the appearance of SCL34A2 is common to xenografts and biopsies prepared from a wider range of

patients with FSHD, we expect that testing for it by immunofluorescence will be useful in diagnostic panels and therapeutic drug screens.

Future studies utilizing our muscle engraftment model of FSHD will include physiological comparisons of engrafted FSHD muscle fibers with controls, as well as deeper analyses of potential phenotypic differences such as full transcriptomic profiling. Quantitative myometry studies of human quadriceps muscle from FSHD patients show a significant impairment, as measured by maximum force of isometric contraction (Statland et al., 2015). Whether this apparent reduction in force is merely due to decreased muscle mass and atrophy or by impaired EC coupling remains unknown. With further improvements, our xenografts should be useful in studies of specific force, fatigability, contraction velocity, and Ca^{2+} signaling on whole muscles or in single fibers.

Nevertheless, our methods are not yet at the point where they can reliably generate TA muscles with nearly 100% human myofibers, nor have we been able so far to isolate individual myofibers from our grafts reproducibly and efficiently enough to sustain single fiber studies. Other limitations include the variability in the number of fibers per graft, the potential for hTERT and CDK4 to evoke changes in gene expression that are independent of the DUX4 program, the absence of an immune component due to our use of NRG mice, and the fact that engraftment minimizes the potential differences in muscle physiology associated with rostro-caudal and dorso-ventral location. Despite these drawbacks, our xenografting methods have produced a model of FSHD that is superior in many ways to the transgenic murine models that have been studied so far, as well as to the use of cultured muscle cells, that inevitably characterize myoblasts or myotubes rather than mature myofibers. Moreover, they are applicable to different clones of FSHD and control cells, as we have recently applied them to the isogeneic C6 and A4 cell lines, derived by the Van der Maarel laboratory (Krom et al., 2012) (Mueller et al., manuscript in preparation).

In conclusion, we show that the xenografts formed by control and FSHD hMPCs in mice treated with iNMES are substantial in size and developmentally mature, composed of human myofibers with minimal contamination of mouse myonuclei. This FSHD model is structurally and molecularly comparable to intact skeletal muscle from patients with FSHD, including elevated expression of *DUX4* and DUX4 targets, and hypomethylation of the D4Z4 RUs. Perhaps most significantly, we have identified SLC34A2 as a quantifiable protein that may serve as a reliable biomarker for FSHD. Our xenograft model can be widely applied, and, because it utilizes hMPCs, which can be expanded nearly without limit, it can be used to create the many mice needed to study the pathogenic mechanism of FSHD and therapeutic strategies for its treatment. We are pursuing such studies now.

4. Materials and methods

4.1. Human muscle biopsies

Muscle biopsies were obtained and FSHD diagnoses were confirmed as reported (Jones et al., 2012).

4.2. Mice

Methods were as described (Sakellariou et al., 2016). Immunocompromised, NOD.Cg-Rag1[tm1Mom]l2rg[tm-Wjl]/SzJ (NRG, Jackson Laboratories, Bar Harbor, ME) mice were used in compliance with the Institutional Animal Care and Use Committee of the University of Maryland, Baltimore. In brief, mice were anesthetized with avertin and their left hindlimbs were subjected to X-irradiation at 25 Gy at 2.2 Gy/min over 11–12 min. For all subsequent steps, mice were anesthetized with 2.5% isoflurane and, for injections, treated with 5 mg/kg carprofen. Six days later, 60 μl of a 0.3 mg/ml solution of cardiotoxin (Sigma Aldrich) was injected along the length of the TA muscle to

promote degeneration. One day later we injected 2×10^6 hMPCs in 60 μl of cell media using a 30G insulin needle, as in our published methods. One week after hMPC injection, mice were subjected to iNMES 3 times per week, as described (Sakellariou et al., 2016). Tissues were collected from engrafted mice 4–5 weeks later. See SI Appendix for details and SI Fig. 1 for a timeline.

4.3. Cells (hMPCs) and cell injection

The immortalized hMPCs were initially prepared from biopsy samples of biceps muscle of patients carrying the FSHD-permissive 4qA allele or their first-degree unaffected relatives (Rahimov et al., 2012). Cells were cloned after retroviral overexpression of CDK4 and immortalized using a retrovirus containing the catalytic subunit of telomerase (hTERT) (Stadler et al., 2011), and expanded in culture prior to injection. Single clones of control and FSHD hMPCs were used in these studies. Cells were cultured on 0.1% gelatin -coated flasks to 85% confluence. Immediately before cell injection, cells were treated with trypsin, pelleted, suspended in 60 μl of media and injected along the length of the TA. See SI Appendix.

4.4. Tissue collection

TAs carrying xenografts were collected 4–5 weeks post-engraftment. Mice were anesthetized and euthanized by cervical dislocation. TAs were dissected, weighed, flash frozen in liquid N_2, and stored at $-80\,°C$. Tissue sections,12–16 μm thick, were mounted on glass microslides (Sakellariou et al., 2016).

4.5. Immunofluorescent labeling

To identify and count human myofibers and myonuclei, we used human-specific antibodies to h-β-spectrin and h-lamin A/C to label the sarcolemmae and nuclear envelopes of human fibers and myonuclei, respectively (Sakellariou et al., 2016). We immunolabeled for desmin to identify muscle tissue and to evaluate sarcomeric organization (Sakellariou et al., 2016). Embryonic myosin (F1.652-s, DSHB) was immunolabeled as an indicator of myofiber immaturity (see Appendix B. Supplemental Methods). To visualize NMJs in the grafts, we used antibodies to synaptophysin (Syp) together with α-bungarotoxin and anti-h-β-spectrin (Sakellariou et al., 2016). We used antibodies to PAX7 (AB_528428, DSHB) on 4% paraformaldehyde-fixed cross sections to identify human satellite cells within the basal lamina, which we labeled with anti-laminin (L9393, Sigma-Aldrich; see Appendix B. Supplemental Methods). Anti-SLC34A2 (#66445, Cell Signaling Technology) was used to label the DUX4-target protein SLC34A2 in grafts and human biopsy cross sections and anti-α-actinin (#A7811, Sigma-Aldrich) was used as a sarcomeric label in human biopsy cross sections. Primary antibody binding was detected with AlexaFluor secondary antibodies (Thermo Fisher Scientific).

4.6. Imaging, morphometry & quantification

Imaging was performed in the UMB confocal microscopy core on an LSM-DUO (Fig. 1a), Nikon CSU-W1 spinning disk (Figs. 1d, 5a, d) or LSM-Meta (Fig. 2b–d) confocal microscope. We used FIJI to quantify fiber number, minimum Feret's diameter, compaction, and central nucleation manually, as described (Sakellariou et al., 2016). We also used FIJI to count fibers expressing SLC34A2 as a percentage of total human fibers within each xenograft.

4.7. Gene expression analysis

Total RNAs were isolated from TAs carrying xenografts with TRIzol (Thermo Fisher), as described (Sharma et al., 2013). The RT-qPCR for *DUX4* and DUX4 target gene expression was as reported (Sharma et al.,

2013). Primer sequences for *ZSCAN4, TRIM43* and *MBD3L2* are published (Geng, 2012). Human *SLC34A2* expression was analyzed with the TaqMan Gene Expression Assay (Thermo Fisher, Assay ID: Hs00197519_m1), using 100 ng cDNA per reaction (generated by iScript cDNA Synthesis Kit, BioRad) and SsoAdvanced Universal Probe Sumermix (BioRad) with the following PCR program: $(1 \times)$ 95 °C, 30 s, $(40 \times)$ 95 °C, 10 s and 60 °C, 40 s.

4.8. Methylation analysis

Genomic DNA of immortalized hMPCs was isolated with the Wizard genomic DNA kit (Promega) as per manufacturer's instructions. Genomic DNA of TAs carrying xenografts was isolated from the organic phase of TRIzol/chloroform extracts after removal of the aquatic phase containing total RNAs (Sharma et al., 2013). BSS for the 4qA allele (BSSA) (Jones et al., 2014) and the 4qB allele (BSSB) was as described (Calandra et al., 2016).

4.9. Statistical analysis

We used unpaired *t*-tests with Welch's correction for statistical analyses of fiber number and TA weight. Tests of fiber diameter and compaction used One-way ANOVA with Tukey's multiple comparisons test. Mann-Whitney *U* tests were used for gene expression data and percent of fibers expressing SLC34A2. We used a Two-way ANOVA with Bonferroni's multiple comparisons test for analyses of central nucleation. Additional statistical methods are given in the text. All statistics were performed with GraphPad.

Appendix A. Supplementary data

Supplementary data to this article can be found online at https://doi.org/10.1016/j.expneurol.2019.113011.

References

Balog, J., et al., 2012. Correlation analysis of clinical parameters with epigenetic modifications in the DUX4 promoter in FSHD. Epigenetics 7 (6), 579–584.

van den Boogaard, M.L., et al., 2016. Mutations in DNMT3B modify epigenetic repression of the D4Z4 repeat and the penetrance of facioscapulohumeral dystrophy. Am. J. Hum. Genet. 98 (5), 1020–1029.

Bosnakovski, D., et al., 2017. Muscle pathology from stochastic low level DUX4 expression in an FSHD mouse model. Nat. Commun. 8 (1), 550.

Briguet, A., Courdier-Fruh, I., Foster, M., Meier, T., Magyar, J.P., 2004. Histological parameters for the quantitative assessment of muscular dystrophy in the mdx-mouse. Neuromuscul. Disord. 14 (10), 675–682.

Calandra, P., et al., 2016. Allele-specific DNA hypomethylation characterises FSHD1 and FSHD2. J. Med. Genet. 53 (5), 348–355.

Capetanaki, Y., Bloch, R.J., Kouloumenta, A., Mavroidis, M., Psarras, S., 2007. Muscle intermediate filaments and their links to membranes and membranous organelles. Exp. Cell Res. 313 (10), 2063–2076.

Chen, J.C., et al., 2016. Morpholino-mediated knockdown of DUX4 toward facioscapulohumeral muscular dystrophy therapeutics. Mol. Ther. 24 (8), 1405–1411.

Clapp, J., et al., 2007. Evolutionary conservation of a coding function for D4Z4, the tandem DNA repeat mutated in Facioscapulohumeral muscular dystrophy. Am. J. Hum. Genet. 81 (2), 264–279.

Daxinger, L., Tapscott, S.J., van der Maarel, S.M., 2015. Genetic and epigenetic contributors to FSHD. Curr. Opin. Genet. Dev. 33, 56–61.

van Deutekom, J.C., et al., 1993. FSHD associated DNA rearrangements are due to deletions of integral copies of a 3.2 kb tandemly repeated unit. Hum. Mol. Genet. 2 (12), 2037–2042.

Dixit, M., et al., 2007. DUX4, a candidate gene of facioscapulohumeral muscular dystrophy, encodes a transcriptional activator of PITX1. Proc. Natl. Acad. Sci. U. S. A. 104 (46), 18157–18162.

Ehrhardt, J., Brimah, K., Adkin, C., Partridge, T., Morgan, J., 2007. Human muscle precursor cells give rise to functional satellite cells in vivo. Neuromuscul. Disord. 17 (8), 631–638.

Emde, B., Heinen, A., Godecke, A., Bottermann, K., 2014. Wheat germ agglutinin staining as a suitable method for detection and quantification of fibrosis in cardiac tissue after myocardial infarction. European journal of histochemistry: EJH 58 (4), 2448.

Fakhfakh, R., Lamarre, Y., Skuk, D., Tremblay, J.P., 2012a. Losartan enhances the success of myoblast transplantation. Cell Transplant. 21 (1), 139–152.

Fakhfakh, R., Lee, S.J., Tremblay, J.P., 2012b. Administration of a soluble activin type IIB receptor promotes the transplantation of human myoblasts in dystrophic mice. Cell Transplant. 21 (7), 1419–1430.

Ferreboeuf, M., et al., 2014. DUX4 and DUX4 downstream target genes are expressed in fetal FSHD muscles. Hum. Mol. Genet. 23 (1), 171–181.

Gabriels, J., et al., 1999. Nucleotide sequence of the partially deleted D4Z4 locus in a patient with FSHD identifies a putative gene within each 3.3 kb element. Gene 236 (1), 25–32.

Geng, L.N., Tyler, A.E., Tapscott, S.J., 2011. Immunodetection of human double homeobox 4. Hybridoma 30 (2), 125–130.

Geng, L.N., et al., 2012. DUX4 activates germline genes, retroelements, and immune mediators: implications for facioscapulohumeral dystrophy. Dev. Cell 22 (1), 38–51.

Himeda, C.L., et al., 2014. Myogenic enhancers regulate expression of the facioscapulohumeral muscular dystrophy-associated DUX4 gene. Mol. Cell. Biol. 34 (11), 1942–1955.

Himeda, C.L., Jones, T.I., Jones, P.L., 2016. CRISPR/dCas9-mediated transcriptional inhibition ameliorates the epigenetic dysregulation at D4Z4 and represses DUX4-fl in FSH muscular dystrophy. Mol. Ther. 24 (3), 527–535.

Himeda, C.L., et al., 2018. Identification of epigenetic regulators of DUX4-fl for targeted therapy of facioscapulohumeral muscular dystrophy. Mol. Ther. 26 (7), 1797–1807.

Homma, S., et al., 2012. A unique library of myogenic cells from facioscapulohumeral muscular dystrophy subjects and unaffected relatives: family, disease and cell function. Eur. J. Hum. Genet. 20 (4), 404–410.

Jagannathan, S., et al., 2016. Model systems of DUX4 expression recapitulate the transcriptional profile of FSHD cells. Hum. Mol. Genet. 25 (20), 4419–4431.

Jones, T., Jones, P.L., 2018. A Cre-inducible DUX4 transgenic mouse model for investigating facioscapulohumeral muscular dystrophy. PLoS One 13 (2), e0192657.

Jones, T.I., et al., 2012. Facioscapulohumeral muscular dystrophy family studies of DUX4 expression: evidence for disease modifiers and a quantitative model of pathogenesis. Hum. Mol. Genet. 21 (20), 4419–4430.

Jones, T.I., et al., 2014. Identifying diagnostic DNA methylation profiles for facioscapulohumeral muscular dystrophy in blood and saliva using bisulfite sequencing. Clin. Epigenetics 6 (1), 23.

Jones, T.I., et al., 2015. Individual epigenetic status of the pathogenic D4Z4 macrosatellite correlates with disease in facioscapulohumeral muscular dystrophy. Clin. Epigenetics 7, 37.

Krom, Y.D., et al., 2012. Generation of isogenic D4Z4 contracted and noncontracted immortal muscle cell clones from a mosaic patient: a cellular model for FSHD. Am. J. Pathol. 181 (4), 1387–1401.

Krom, Y.D., et al., 2013. Intrinsic epigenetic regulation of the D4Z4 macrosatellite repeat in a transgenic mouse model for FSHD. PLoS Genet. 9 (4), e1003415.

Lemmers, R.J., et al., 2002. Facioscapulohumeral muscular dystrophy is uniquely associated with one of the two variants of the 4q subtelomere. Nat. Genet. 32 (2), 235–236.

Lemmers, R.J., et al., 2010. A unifying genetic model for facioscapulohumeral muscular dystrophy. Science (New York, N.Y.) 329 (5999), 1650–1653.

van Overveld, P.G., et al., 2003. Hypomethylation of D4Z4 in 4q-linked and non-4q-linked facioscapulohumeral muscular dystrophy. Nat. Genet. 35 (4), 315–317.

Quenneville, S.P., et al., 2007. Autologous transplantation of muscle precursor cells modified with a lentivirus for muscular dystrophy: human cells and primate models. Mol. Ther. 15 (2), 431–438.

Rahimov, F., et al., 2012. Transcriptional profiling in facioscapulohumeral muscular dystrophy to identify candidate biomarkers. Proc. Natl. Acad. Sci. U. S. A. 109 (40), 16234–16239.

Ricci, G., Zatz, M., Tupler, R., 2014. Facioscapulohumeral muscular dystrophy: more complex than it appears. Curr. Mol. Med. 14 (8), 1052–1068.

Roche, J.A., et al., 2010. Extensive mononuclear infiltration and myogenesis characterize recovery of dysferlin-null skeletal muscle from contraction-induced injuries. Am J Physiol Cell Physiol 298 (2), C298–C312.

Roche, J.A., Ru, L.W., Bloch, R.J., 2012. Distinct effects of contraction-induced injury in vivo on four different murine models of dysferlinopathy. J. Biomed. Biotechnol. 2012, 134031.

Roche, J.A., et al., 2015. Myofiber damage precedes macrophage infiltration after in vivo injury in dysferlin-deficient a/J mouse skeletal muscle. Am. J. Pathol. 185 (6), 1686–1698.

Sakellariou, P., et al., 2016. Neuromuscular electrical stimulation promotes development in mice of mature human muscle from immortalized human myoblasts. Skelet. Muscle 6, 4.

Sharma, V., Harafuji, N., Belayew, A., Chen, Y.W., 2013. DUX4 differentially regulates transcriptomes of human rhabdomyosarcoma and mouse C2C12 cells. PLoS One 8 (5), e64691.

Snider, L., et al., 2010. Facioscapulohumeral dystrophy: incomplete suppression of a retrotransposed gene. PLoS Genet. 6 (10), e1001181.

Spangenburg, E.E., Pratt, S.J.P., Wohlers, L.M., Lovering, R.M., 2011. Use of BODIPY (493/503) to visualize intramuscular lipid droplets in skeletal muscle. J. Biomed. Biotechnol. 2011, 598358.

Stadler, G., et al., 2011. Establishment of clonal myogenic cell lines from severely affected dystrophic muscles - CDK4 maintains the myogenic population. Skelet. Muscle 1 (1), 12.

Statland, J.M., et al., 2015. Muscle pathology grade for facioscapulohumeral muscular dystrophy biopsies. Muscle Nerve 52 (4), 521–526.

Su, A.I., et al., 2004. A gene atlas of the mouse and human protein-encoding transcriptomes. Proc. Natl. Acad. Sci. U. S. A. 101 (16), 6062–6067.

Tassin, A., et al., 2013. DUX4 expression in FSHD muscle cells: how could such a rare protein cause a myopathy? J. Cell. Mol. Med. 17 (1), 76–89.

Tupler, R., Gabellini, D., 2004. Molecular basis of facioscapulohumeral muscular dystrophy. Cell. Mol.Life Sci. 61 (5), 557–566.

Wallace, L.M., et al., 2011. DUX4, a candidate gene for facioscapulohumeral muscular dystrophy, causes p53-dependent myopathy in vivo. Ann. Neurol. 69 (3), 540–552.

Wallace, L.M., et al., 2012. RNA interference inhibits DUX4-induced muscle toxicity in vivo: implications for a targeted FSHD therapy. Mol. Ther. 20 (7), 1417–1423.

Xu, H., et al., 2014. Dux4 induces cell cycle arrest at G1 phase through upregulation of p21 expression. Biochem. Biophys. Res. Commun. 446 (1), 235–240.

Yao, Z., et al., 2014. DUX4-induced gene expression is the major molecular signature in FSHD skeletal muscle. Hum. Mol. Genet. 23 (20), 5342–5352.

Zeng, W., et al., 2009. Specific loss of histone H3 lysine 9 trimethylation and HP1gamma/cohesin binding at D4Z4 repeats is associated with facioscapulohumeral dystrophy (FSHD). PLoS Genet. 5 (7), e1000559.

Zhang, Y., et al., 2014. Human skeletal muscle xenograft as a new preclinical model for muscle disorders. Hum. Mol. Genet. 23 (12), 3180–3188.